Driving Force of the Initial Step in Electrochemical Pt(111) Oxidation

Timo Fuchs, Valentín Briega-Martos, Jan O. Fehrs, Canrong Qiu, Marta Mirolo, Chentian Yuan, Serhiy Cherevko, Jakub Drnec, Olaf M. Magnussen, and David A. Harrington

2023

The final publication is available at:

https://doi.org/10.1021/acs.jpclett.3c00520

doi: 10.1021/acs.jpclett.3c00520

Driving Force of the Initial Step in Electrochemical Pt(111) Oxidation

Timo Fuchs,[†] Valentín Briega-Martos,[‡] Jan O. Fehrs,[†] Canrong Qiu,[†] Marta Mirolo,[¶] Chentian Yuan,[§] Serhiy Cherevko,[‡] Jakub Drnec,[¶] Olaf M. Magnussen,[†] and David A. Harrington*[,§]

[†]*Institut für Experimentelle und Angewandte Physik, Christian-Albrechts-Universität zu Kiel, Olshausenstr. 40, 24098 Kiel, Germany*

[‡]*Forschungszentrum Jülich GmbH, Helmholtz Institute Erlangen-Nürnberg for Renewable Energy (IEK-11), Erlangen 91058, Germany*

[¶]*Experimental division, European Synchrotron Radiation Facility, 71 Avenue des Martyrs, 38000 Grenoble, France*

[§]*Chemistry Department, University of Victoria, Victoria, British Columbia, V8W 2Y2, Canada*

E-mail: dharr@uvic.ca

Abstract

The first step of electrochemical surface oxidation is extraction of a metal atom from its lattice site to a location in a growing oxide. Here we show by fast simultaneous electrochemical and *in situ* high-energy surface X-ray diffraction measurements that the initial extraction of Pt atoms from Pt(111) is a fast, potential-driven process, whereas charge transfer for the related formation of adsorbed oxygen-containing species occurs on a much slower time scale and is evidently uncoupled from the extraction process. It is concluded that potential plays a key independent role in electrochemical surface oxidation.

TOC Graphic

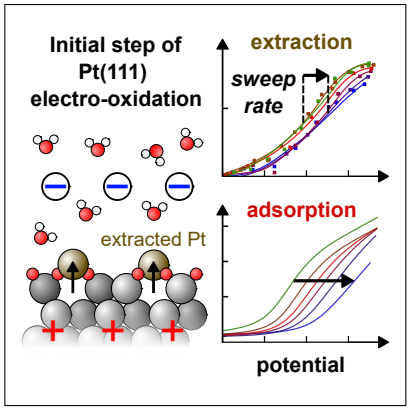

Keywords

electrochemistry, high-energy surface X-ray diffraction, metal oxidation, Pt(111), place-exchange

Electrochemical oxidation is of key importance for the stability of metals in aqueous environments. In its initial stage metal atoms are extracted from the surface layer and moved to a position in the emerging oxide lattice. The direct observation of this fundamental step is difficult for base metals that actively corrode, because of the difficulty of producing clean surfaces and the speed of the oxidation. However, use of noble metals allows preparation of clean surfaces that are well-defined on the atomic scale, and for which *in situ* methods can directly observe this extraction. Here we present the first fast measurements that simultanously detect the initial extraction of Pt atoms from Pt(111) and the accompanying electrochemical current due to the formation of oxygen species on the surface. We use high-energy surface X-ray diffraction (HESXRD) measurements during fast cyclic voltammetry to reveal that the extraction proceeds much faster than the charge transfer. Electrochemical oxidation is therefore not coupled to the uptake of oxygen species and thus is inherently different from gas-phase thermal oxidation.

Platinum in perchloric acid electrolyte is arguably the best studied noble metal in terms of its initial oxidation, and the most stable Pt(111) surface allows the closest control over this process. A place-exchange phenomenon, in which an adsorbed oxygen or OH species exchanges places with a surface metal atom, was first suggested as the initial step in gas-phase oxidation,[1] and widely assumed for electrochemical Pt oxidation.[2] The electrochemical exchange process was proposed to be flipping of dipoles driven by an electric field,[3] though the Tafel-like potential dependence was also consistent with a charge-transfer reaction,[4,5] providing an alternative hypothesis. However, most studies were on polycrystalline surfaces and did not directly detect the extraction. Indirect evidence was first obtained by observations of Pt surface restructuring after oxidation-reduction cycles using low energy electron diffraction[6] and *in situ* scanning tunneling microscopy.[7,8]

Direct evidence of the place-exchange oxidation event was first gathered using *in situ* surface X-ray diffraction (SXRD) by You et al.,[9] who found lifting of Pt surface atoms by 2 Å at potentials above about 1V vs. the reversible hydrogen electrode (RHE), and a return of these atoms to their original locations when the oxide was reduced, provided the potential did not exceed 1.18 V.[10] The same group also showed that the sharp reduction in X-ray intensity caused by the place exchange occurs in the same potential region (0.9 – 1.2 V) where cyclic voltammograms exhibit a peak usually referred to as the "O_{ads}" peak.[10] This peak, shown in Figure 1a, has more traditionally been assigned to the oxidation of adsorbed OH to adsorbed O without place exchange,[11] but evidently both processes are occurring at the same time.

Improvements in synchrotron and X-ray detector technology allowed for better atom localization in more recent SXRD studies.[13–19] Slight buckling of the Pt surface atoms was shown just before the oxide peak.[14] The location of the extracted Pt atom (Pt_{ex}) was refined to 2.41 $\pm$ 0.02 Å above its original location at 1.17 V, with some evidence for the oxygen atom underneath the extracted Pt atom.[15,18] Density functional theory (DFT) calculations[20–22] suggest that a critical local coverage of nearby oxygen surface atoms is required for the extraction. These atoms and interactions with water may stabilize the extracted Pt atom without the O atom underneath,[20] and the actual O insertion into the Pt lattice may occur afterward.[21] Accordingly, we refer to the movement of the Pt atom as extraction rather than exchange.

Up to now, the Pt extraction process was studied under quasi-stationary conditions or at slow potential sweep rates ($\leq$ 20 mV s^{-1}).[9,10,15–20] Under these conditions, the decrease in X-ray intensity starts approximately at potentials near the maximum of the O_{ads} peak. This is consistent with the required production of the critical number of stabilizing O atoms in the early part of the CV peak before the extraction is initiated.

In this work, use of high energy X-rays (77 keV), a large-area 2-D detector with a time resolution of 25 ms, and an SXRD cell that allows single crystal electrochemistry under carefully optimized conditions,[23] enables measurements at much faster sweep rates.

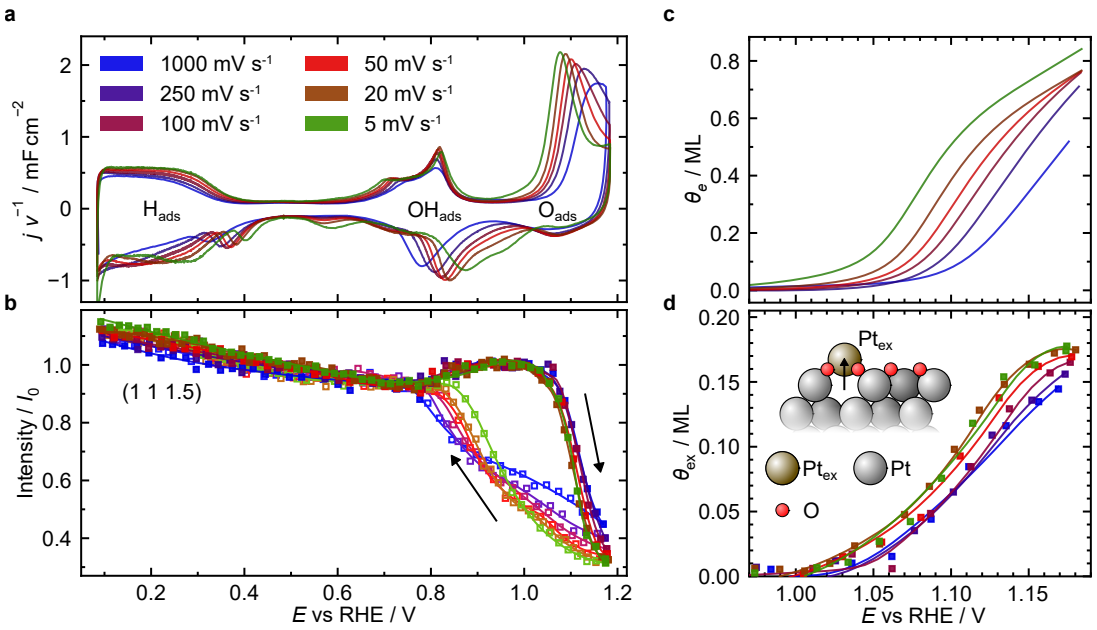

Figure 1: Electrochemical and X-ray diffraction response of Pt(111) as a function of sweep rate. (a) Cyclic voltammograms of Pt(111) in 0.1 M $HClO_4$. Current densities have been normalized by dividing by the sweep rate. (b) X-ray intensity at the (1 1 1.5) anti-Bragg position, normalized to the intensity at 0.97 V. (Indexing is relative to a hexagonal unit cell.[12]) Above 1 V the intensity decreases as Pt extraction occurs. (c) Integrated charge density in the oxide peak, obtained from the voltammograms after double layer charge correction and expressed in electrons per surface Pt atom. (d) Coverage of extracted Pt atoms determined from the X-ray intensity. The coverage during the reverse sweep is shown in Figure S6. Curve shifts with potential may be judged from fits shown in Figure S2.

Care was taken to limit potentials to below 1.18 V to avoid producing other types of oxide species and permanently restructuring the surface.[19,24–27] Dissolution is negligible compared to oxidation under these conditions.[20,28,29]

Simultaneous current and X-ray voltammograms at sweep rates up to 1000 mV s^{-1} are shown in Figure 1. The sweep rate variation in the O_{ads} peak and the X-ray intensity are dramatically different, establishing that the underlying processes are not directly coupled.

In the regime of the underpotential adsorption/desorption of hydrogen (0.0 – 0.4 V) and OH adsorption/desorption (0.6 – 0.9 V) the voltammetry peaks do not shift with sweep rate, which is consistent with their known fast kinetics. However, there is a shift in the O_{ads} voltammetry peak with sweep rate, showing that the charge-transfer process is kinetically slow on this timescale, as previously observed.[11,30] The Pt extraction, measured by the decrease in X-ray intensity above 0.95 V, is much faster than the electron transfer, with the intensity shifting by less than 20 mV while the O_{ads} peak shifts by about 80 mV. For the fastest sweep rate here, the extraction occurs before significant charge has passed in the O_{ads} peak, which may suggest that the species being produced in this peak is not a prerequisite to the extraction, or is required only in very small amounts. However, we did not attain high enough sweep rates to check if extraction could be initiated before the peak process.

To better understand the extraction process occurring in Figure 1b, the coverages of the extracted atoms, θ_{ex}, were determined by carrying out a detailed structural study using HES-XRD.[20,31] Crystal truncation rods were measured at 20 mV intervals from 1.01 to 1.17 V, Figure 2a.

Fits of these data by the structural model shown in Figure 2b give a relationship between the coverage of the extracted Pt atoms and the normalized intensity at (1 1 1.5) (Figure 2c).

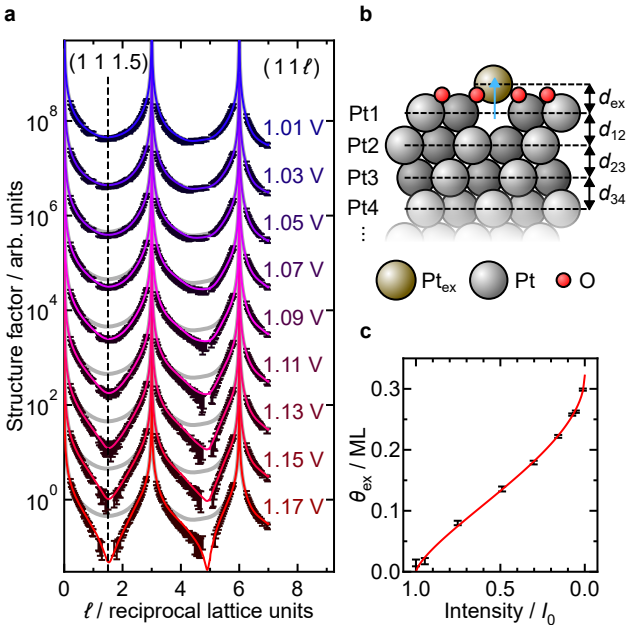

Figure 2: Structural analysis of extracted Pt atoms by HESXRD. (a) (1 1 ℓ) crystal truncation rods, measured at different potentials. The full data sets are given in supporting information Figure S1. Gray lines are the fit at 1.01 V as a reference. The vertical dashed line indicates the (1 1 1.5) position, used for the intensity measurements during potential sweeps. (b) Schematic illustration of the model used for the quantitative fits of the HESXRD data. (c) Relationship between the coverage of extracted Pt atoms θ_{ex} and the normalized (1 1 1.5) intensity.

This relationship was parameterized (see methods section of the supporting information), and used to determine the coverages during the fast sweeps from the measured intensities, with the results shown in Figure 1d.

The fast extraction process is initiated at a nearly constant potential and depends very little on sweep rate, which shows that the extraction is driven by potential, independently of the adsorbed species around it. The maximum coverage of extracted atoms is 0.18 ML. For comparison, the integrated charge through the O_{ads} peak is expressed as a coverage and denoted θ_e,[5,32] the number of electrons per surface atom (Figure 1c). Its maximum value is 0.8 ML. A high ratio of electrons to extracted Pt atoms was already noted in 1994[9,10] for slow experiments, and is incompatible with a simple stoichiometric reaction producing an oxidized Pt(I) or Pt(II) species from adsorbed OH or O. If the extraction process contributed one or more electrons per Pt_{ex} to the anodic current in the O_{ads} peak, it would lead to an observable feature in the peak, especially at the highest sweep rates. The lack of such a feature further emphasizes the uncoupled nature of the two parallel processes, and shows that the oxidation has a complicated mechanism.

The small dependence of the extraction process on sweep rate argues for a process where Pt surface atoms and extracted Pt atoms are in quasi-equilibrium, controlled by the potential. In the simplest model with no interactions between the extracted Pt atoms, the resulting equilibrium coverage would be given by the electrochemical Langmuir isotherm. The coverage vs. potential relationship on the forward sweep fits well to this model, as shown in the supporting information, Figure S4.

However, for an equilibrium process alone, the coverage would be expected to be the same function of potential on the reverse sweep, but this is not observed. For the fastest sweep rate, the coverage decreases more rapidly, but already after 50 ms (two data points in Figure 1b) an irreversible process is apparent that prevents return of the extracted atom. The DFT studies of extraction[20,21] hint at an explanation as they show that a critical coverage of 0.6 – 0.7 ML adsorbed oxygen atoms, or about 3 – 4 oxygen atoms per extracted atom, can stabilize the Pt_{ex}. At the onset of extraction, where the O_{ads} coverage is not sufficient, oxygen atoms may move on the surface to create a high local coverage that stabilizes and traps the extracted Pt atoms, preventing their return. The DFT studies show that water molecules play a role in stabilization as well, but do not explicitly consider stabilization by adsorbed OH, which may also play a role. In any case, there is a high enough local coverage of stabilizing oxygenated species (adsorbed OH, O and water) to explain the irreversibility of the extraction process. This trapping by oxygenated species may also explain why the cathodic peak corresponding to the anodic O_{ads} peak has much less charge. On the reverse sweep, the extracted

atoms are not returned to their original sites until more negative potentials between 0.7 and 1.0 V where OH species are removed from the surface. Evidently, the removal of the stabilizing species enables the return of the Pt_{ex} atoms to their original sites. The sweep rate dependence shows that the return is a kinetically controlled process, similar to the reduction current (Figure 1b). The slower reduction of O to OH is rate limiting and enables the Pt motion.

Quantitative kinetic modeling requires specific assumptions about the interactions between the extracted atoms and adsorbed species on the surface and was not attempted here, as both the coverages and the nature of the adsorbed species are uncertain. The O_{ads} peak has variously been attributed to adsorption of O or OH or their interconversion,[11,21,32–35] or production of a species with two O atoms.[24,36]

Potential step experiments further confirm that there is a fast extraction process with potential dependence similar to that in the voltammograms. Figure S4 shows the initial coverages resulting from successive potential steps from a potential in the double layer region (0.47 V) to the indicated potentials. The coverage rapidly changes during the step and after 2 s, the coverage is nearly the same as in the forward sweeps at the same potential. This fast process is followed by a much slower increase in coverage, which will be analyzed elsewhere.

In summary, the experiments here show that the initial stage of metal electrooxidation is a complex process where the potential itself plays a decisive role. Extraction of Pt atoms occurs in a fast process in which the coverage of the extracted atoms is determined by the potential and is largely independent of the coverage of adsorbed oxygenated species on the Pt surface. Specifically, it is uncoupled from the slower adsorption and surface reactions of adsorbed species associated with the voltammetry peak occurring simultaneously. Thus, the extraction is driven by potential rather than oxygen coverage. Consequently, electrochemical oxidation may be inherently different from gas phase oxidation, which is driven solely by the oxygen's chemical potential. In gas phase oxidation, the electric field cannot be changed independently of the coverage, as it is the sum of the local fields of the adsorbed species. A proper description of electrochemical oxidation processes therefore requires going beyond solid-vacuum interface models, and must explicitly recognize the role of the electrochemical double layer.

Author Information
Corresponding Author
David A. Harrington – Department of Chemistry, University of Victoria, Victoria, BC, Canada V8W 2Y2.
orcid: 0000-0002-9901-6795 Email: dharr@uvic.ca.
Complete contact information is available at https://pubs.acs.org/doi/10.1021/XXXX

Notes
The authors declare no competing financial interest.

Acknowledgement The HESXRD experiments were performed on beamline ID31 at the European Synchrotron Radiation Facility (ESRF), Grenoble, France. We are grateful to H. Isern at the ESRF for providing assistance in using beamline ID31. Funding is acknowledged from the Natural Sciences and Engineering Research Council of Canada (NSERC) via grant RGPIN-2017-04045, the Deutsche Forschungsgemeinschaft (DFG) via grant 418603497, and the German Federal Ministry of Education and Research (BMBF) via project 05K19FK3.

Supporting Information Available
The Supporting Information is available free of charge at https://pubs.acs.org/doi/10.1021/XXXX

- Methods, Relationship of extracted coverages to potential, Cyclic voltammograms and potential step transients (PDF)

References

(1) Lanyon, M. A. H.; Trapnell, B. M. W. The interaction of oxygen with clean metal surfaces. *Proc. Roy. Soc. London. Ser. A. Math. Phys. Sci.* **1955**, *227*, 387–399.

(2) Conway, B. E. Electrochemical oxide film formation at noble metals as a surface-

chemical process. *Prog. in Surf. Sci.* **1995**, *49*, 331–452.

(3) Conway, B. E.; Barnett, B.; Angerstein-Kozlowska, H.; Tilak, B. V. A surface-electrochemical basis for the direct logarithmic growth law for initial stages of extension of anodic oxide films formed at noble metals. *J. Chem. Phys.* **1990**, *93*, 8361–8373.

(4) van der Geest, M. E.; Dangerfield, N. J.; Harrington, D. A. An ac voltammetry study of Pt oxide growth. *J. Electroanal. Chem.* **1997**, *420*, 89–100.

(5) Björling, A.; Feliu, J. M. Electrochemical surface reordering of Pt(111): A quantification of the place-exchange process. *J. Electroanal. Chem.* **2011**, *662*, 17–24.

(6) Wagner, F.; Ross, P. LEED spot profile analysis of the structure of electrochemically treated Pt(100) and Pt(111) surfaces. *Surf. Sci.* **1985**, *160*, 305 – 330.

(7) Itaya, K.; Sugawara, S.; Sashikata, K.; Furuya, N. In situ scanning tunneling microscopy of platinum (111) surface with the observation of monoatomic steps. *J. Vac. Sci. Technol. A* **1990**, *8*, 515.

(8) Sashikata, K. In situ electrochemical scanning tunneling microscopy of single-crystal surfaces of Pt(111), Rh(111), and Pd(111) in aqueous sulfuric acid solution. *J. Vac. Sc. Techn. B* **1991**, *9*, 457.

(9) You, H.; Zurawski, D. J.; Nagy, Z.; Yonco, R. M. In-situ x-ray reflectivity study of incipient oxidation of Pt(111) surface in electrolyte solutions. *J. Chem. Phys.* **1994**, *100*, 4699–4702.

(10) Nagy, Z.; You, H. Applications of surface X-ray scattering to electrochemistry problems. *Electrochim. Acta* **2002**, *47*, 3037–3055.

(11) Gómez-Marín, A. M.; Clavilier, J.; Feliu, J. M. Sequential Pt(111) oxide formation in perchloric acid: An electrochemical study of surface species inter-conversion. *J. Electroanal. Chem.* **2013**, *688*, 360–370.

(12) Wang, J.; Ocko, B.; Davenport, A.; Isaacs, H. In situ X-ray-diffraction and -reflectivity studies of the Au(111)/electrolyte interface: reconstruction and anion adsorption. *Phys. Rev. B* **1992**, *46*, 10321–10338.

(13) Kondo, T.; Masuda, T.; Aoki, N.; Uosaki, K. Potential-dependent structures and potential-induced structure changes at Pt(111) single-crystal electrode/sulfuric and perchloric acid interfaces in the potential region between hydrogen underpotential deposition and surface oxide formation by *In Situ* surface X-ray scattering. *J. Phys. Chem. C* **2016**, *120*, 16118–16131.

(14) Liu, Y.; Barbour, A.; Komanicky, V.; You, H. X-ray crystal truncation rod studies of surface oxidation and reduction on Pt(111). *J. Phys. Chem. C* **2016**, *120*, 16174–16178.

(15) Drnec, J.; Ruge, M.; Reikowski, F.; Rahn, B.; Carlà, F.; Felici, R.; Stettner, J.; Magnussen, O. M.; Harrington, D. A. Initial stages of Pt(111) electrooxidation: dynamic and structural studies by surface X-ray diffraction. *Electrochim. Acta* **2017**, *224*, 220–227.

(16) Drnec, J.; Harrington, D. A.; Magnussen, O. M. Electrooxidation of Pt(111) in acid solution. *Curr. Op. Electrochem.* **2017**, *4*, 69–75.

(17) Drnec, J.; Ruge, M.; Reikowski, F.; Rahn, B.; Carla, F.; Felici, R.; Stettner, J.; Magnussen, O. M.; Harrington, D. A. Pt oxide and oxygen reduction at Pt(111) studied by surface X-ray diffraction. *Electrochem. Comm.* **2017**, *84*, 50–52.

(18) Ruge, M.; Drnec, J.; Rahn, B.; Reikowski, F.; Harrington, D.; Carlà, F.; Felici, R.; Stettner, J.; Magnussen, O. Electrochemical oxidation of smooth

and nanoscale rough Pt(111): An in situ surface X-ray scattering study. *J. Electrochem. Soc* **2017**, *164*, H608–H614.

(19) Jacobse, L.; Vonk, V.; McCrum, I. T.; Seitz, C.; Koper, M. T.; Rost, M. J.; Stierle, A. Electrochemical oxidation of Pt(111) beyond the place-exchange model. *Electrochim. Acta* **2022**, *407*, 139881.

(20) Fuchs, T.; Drnec, J.; Calle-Vallejo, F.; Stubb, N.; Sandbeck, D. J. S.; Ruge, M.; Cherevko, S.; Harrington, D. A.; Magnussen, O. M. Structure dependency of the atomic-scale mechanisms of platinum electro-oxidation and dissolution. *Nat. Catal.* **2020**, *3*, 754–761.

(21) Eslamibidgoli, M. J.; Eikerling, M. H. Atomistic mechanism of Pt extraction at oxidized surfaces: Insights from DFT. *Electrocatalysis* **2016**, *7*, 345–354.

(22) Fantauzzi, D.; Mueller, J. E.; Sabo, L.; van Duin, A. C. T.; Jacob, T. Surface buckling and subsurface oxygen: atomistic insights into the surface oxidation of Pt(111). *ChemPhysChem.* **2015**, *16*, 2797–2802.

(23) Magnussen, O. M.; Krug, K.; Ayyad, A. H.; Stettner, J. In situ diffraction studies of electrode surface structure during gold electrodeposition. *Electrochim. Acta* **2008**, *53*, 3449–3458.

(24) Huang, Y.-F.; Kooyman, P. J.; Koper, M. T. M. Intermediate stages of electrochemical oxidation of single-crystalline platinum revealed by in situ Raman spectroscopy. *Nature Communications* **2016**, *7*.

(25) Ruge, M.; Drnec, J.; Rahn, B.; Reikowski, F.; Harrington, D. A.; Carlà, F.; Felici, R.; Stettner, J.; Magnussen, O. M. Structural reorganisation of Pt(111) electrodes by electrochemical oxidation and reduction. *J. Am. Chem. Soc.* **2017**, *139*, 4532–4539.

(26) Jacobse, L.; Huang, Y.-F.; Koper, M. T. M.; Rost, M. J. Correlation of surface site formation to nanoisland growth in the electrochemical roughening of Pt(111). *Nat. Mater.* **2018**, *17*, 277–282.

(27) Mascaró, F. V.; McCrum, I. T.; Koper, M. T. M.; Rost, M. J. Nucleation and growth of dendritic islands during platinum oxidation-reduction cycling. *J. Electrochem. Soc.* **2022**, *169*, 112506.

(28) Sandbeck, D. J.; Brummel, O.; Mayrhofer, K. J.; Libuda, J.; Katsounaros, I.; Cherevko, S. Dissolution of platinum single crystals in acidic medium. *ChemPhysChem* **2019**, *20*, 2997–3003.

(29) Lopes, P. P.; Strmcnik, D.; Tripkovic, D.; Connell, J. G.; Stamenkovic, V.; Markovic, N. M. Relationships between atomic level surface structure and stability/activity of platinum surface atoms in aqueous environments. *ACS Catal.* **2016**, *6*, 2536–2544.

(30) Gómez-Marín, A. M.; Feliu, J. M. Oxide growth dynamics at Pt(111) in absence of specific adsorption: A mechanistic study. *Electrochim. Acta* **2013**, *104*, 367–377.

(31) Gustafson, J.; Shipilin, M.; Zhang, C.; Stierle, A.; Hejral, U.; Ruett, U.; Gutowski, O.; Carlsson, P.-A.; Skoglundh, M.; Lundgren, E. High-energy surface X-ray diffraction for fast surface structure determination. *Science* **2014**, *343*, 758–761.

(32) Gómez-Marín, A. M.; Feliu, J. M. Pt(111) surface disorder kinetics in perchloric acid solutions and the influence of specific anion adsorption. *Electrochim. Acta* **2012**, *82*, 558–569.

(33) Tian, F.; Jinnouchi, R.; Anderson, A. B. How Potentials of Zero Charge and Potentials for Water Oxidation to OH(ads) on Pt(111) Electrodes Vary With Coverage. *J. of Phys. Chem. C* **2009**, *113*, 17484–17492.

(34) Bondarenko, A. S.; Stephens, I. E. L.; Hansen, H. A.; Pérez-Alonso, F. J.; Tripkovic, V.; Johansson, T. P.; Rossmeisl, J.; Nørskov, J. K.; Chorkendorff, I. The Pt(111)/electrolyte interface under oxygen reduction reaction conditions: An electrochemical impedance spectroscopy study. *Langmuir* **2011**, *27*, 2058–2066.

(35) Sugimura, F.; Sakai, N.; Nakamura, T.; Nakamura, M.; Ikeda, K.; Sakai, T.; Hoshi, N. In situ observation of Pt oxides on the low index planes of Pt using surface enhanced Raman spectroscopy. *Phys. Chem. Chem. Phys.* **2017**, *19*, 27570–27579.

(36) Rinaldo, S. G.; Lee, W.; Stumper, J.; Eikerling, M. Mechanistic principles of platinum oxide formation and reduction. *Electrocatalysis* **2014**, *5*, 262–272.

Supporting Information: Driving Force of the Initial Step in Electrochemical Pt(111) Oxidation

Timo Fuchs,[†] Valentín Briega-Martos,[‡] Jan O. Fehrs,[†] Canrong Qiu,[†] Marta Mirolo,[¶] Chentian Yuan,[§] Serhiy Cherevko,[‡] Jakub Drnec,[¶] Olaf M. Magnussen,[†] and David A. Harrington[*,§]

†*Institut für Experimentelle und Angewandte Physik, Christian-Albrechts-Universität zu Kiel, Olshausenstr. 40, 24098 Kiel, Germany*

‡*Forschungszentrum Jülich GmbH, Helmholtz Institute Erlangen-Nürnberg for Renewable Energy (IEK-11), Erlangen 91058, Germany*

¶*Experimental division, European Synchrotron Radiation Facility, 71 Avenue des Martyrs, 38000 Grenoble, France*

§*Chemistry Department, University of Victoria, Victoria, British Columbia, V8W 2Y2, Canada*

E-mail: dharr@uvic.ca

Methods

Experiments were carried out at the ID31 beamline of the European Synchrotron Radiation Facility, and details of the experimental arrangement have been described previously,[S1] with only a brief summary given here. A 7 mm dia. Pt(111) crystal was the working electrode in an inverted hanging meniscus electrochemical cell.[S2] The cell had a Pt foil counter electrode and a Ag|AgCl (3.4 M KCl) reference electrode (Innovative Instruments), but potentials are reported here vs. RHE. The Pt(111) surface was prepared by annealing under a reducing atmosphere of 5 % H_2 and 95 % Ar in an induction furnace at about 1050 °C. The crystal was subsequently transferred to the cell protected by a drop of ultrapure water and was immersed under potential control in 0.1 M $HClO_4$ (Merck suprapur). The potential was controlled by an SP-300 Biologic potentiostat. The solution resistance was determined with an impedance measurement, and then hardware IR compensation was applied with nominal 85 % compensation. An additional 5 % software compensation was applied in the data processing stage. The charge densities in the oxide peak were determined by integrating the current density with respect to time relative to a horizontal baseline determined at the current minimum prior to the oxide peak, and were then converted to electrons per Pt surface atom (θ_e) by dividing by 240.3 µC cm^{-2}, which corresponds to the charge density for one electron per surface atom on a Pt(111) plane.

The incident angle of the 77 keV X-ray beam on the crystal surface was adjusted close to the critical angle of total external reflection of Pt (0.067 °) to maximize the diffraction signal from the (1 1 1.5) reflection (relative to a hexagonal unit cell[S3]). The reflection was detected on a stationary large-area X-ray detector (Dectris Pilatus 2M), which was positioned 79.4 cm behind the Pt(111) crystal, with a time resolution of 25 ms. The diffraction signal was integrated in a rectangular region of 8×35 pixels (horizontal × vertical) on the detector. The background intensity was integrated in two equally sized rectangular regions horizontally adjacent to the reflection and subtracted from the center signal. All X-ray intensities were normalized by the incident beam flux, which was measured with a photodiode pointed at

an Al foil placed in the incident beam. The corrected intensity was converted to structure factor by taking the square root of the intensity normalized to the intensity at 0.97 V. To improve the counting statistics for the two highest sweep rates, the intensities of two (for $250\,\mathrm{mV\,s^{-1}}$) or four (for $1000\,\mathrm{mV\,s^{-1}}$) consecutive cyclic voltammograms were averaged to give the intensity and the corresponding θ_{ex} shown in Figure 1b, d and S6.

For the CTR data set at each potential, 19 non-specular CTRs were measured with a single rocking scan in HESXRD geometry[S4] with a fixed angle of incidence of $0.068\,^{\circ}$. The specular CTR was measured with a second reflectivity rocking scan. Symmetrically equivalent CTRs were averaged to obtain in total 7 non-equivalent CTRs with improved counting statistics and better estimation of the systematic errors of the obtained structure factors.[S1] The CTRs were fitted with the structural model illustrated in Figure 2b, which corresponds to the Pt(111) surface oxide model in the initial stages of oxidation used previously by many groups in the CTR analysis.[S5–S8] A more detailed description of the analysis of the Pt(111) oxide structure together with an error analysis is given in the section below. The results are only briefly summarized here. In the surface oxide model used for the CTR fits, the Pt surface atoms were allowed to vertically relax until the Pt3 layer and their corresponding in-plane and out-of-plane Debye-Waller parameters were fitted. The location of the $\mathrm{Pt_{ex}}$ atom was fixed horizontally above the vacancy from which it originated, and only its height d_{ex} above the vacancy was fitted together with its Debye-Waller parameters. Since dissolution at $< 1.17\,\mathrm{V}$ is below the detection limit of SXRD ($\lessapprox 0.01\,\mathrm{ML}$),[S1,S9,S10] the total number of Pt atoms on the surface was conserved, i.e. for each generated vacancy in the Pt1 layer, one $\mathrm{Pt_{ex}}$ atom is added. X-ray scattering from oxygen is weak compared to Pt, making a precise determination of its location and coverage in the oxide difficult.[S7,S8] However, since O or OH adsorbates clearly are present even before surface oxidation, one monolayer of oxygen was tentatively placed in fcc and hcp hollow site positions, which resembles either atomic oxygen, OH or water in the position predicted by DFT calculations.[S1,S11,S12] Depending on the coverage of oxygen species in the surface structure model (either 1 ML $\mathrm{O_{ads}}$, 0 ML $\mathrm{O_{ads}}$ or 3

O_{ads} for each Pt_{ex}), the Pt_{ex} coverage obtained by the CTR fits varies by about ± 0.026 ML. The CTRs at potentials between 1.01 and 1.17 V are shown together with the CTR fits in Figure S1, and the structural parameters are given in Table S1. The height of the Pt_{ex} at about 2.1 $\pm$ 0.1 Å is in the range of previously reported values[S5–S8] and the overall higher coverage of Pt_{ex} compared to previously reported values is likely caused by the longer cumulative time for oxidation at potentials >1.00 V. The relation between the calculated intensity $I_{1\,1\,1.5} = |F_{1\,1\,1.5}|^2$ at (1 1 1.5) and the coverage of Pt_{ex} atoms obtained from the CTR fits is shown in Figure 2c. This was fitted to the following empirical equation:

$$\theta_{ex}(F_{1\,1\,1.5}) = s \cdot \left(1 - \frac{F_{1\,1\,1.5}}{F_{1\,1\,1.5,\,0.97V}}\right)^{\gamma}$$

yielding $s = 0.322$ ML and $\gamma = 0.722$. $F_{1\,1\,1.5}$ is the measured structure factor at (1 1 1.5) and $F_{1\,1\,1.5,\,0.97V}$ is the structure factor at 0.97 V (before the drop in intensity in the cyclic voltammograms in Figure 1b), which is used as normalization. The coverage of Pt_{ex} atoms in the voltammograms in Figure 1d, S4 and S6 was calculated from the intensity using this relationship. The error bars in these figures only represent the statistical error of the intensity measurement. An additional error of about ± 0.025 ML due to the uncertainty of the oxygen coverage has to be added for a more accurate error of the absolute Pt_{ex} coverage.

The (1 1 1.5) position was chosen for the dynamic cycling study because it is most sensitive to the coverage of the the extracted Pt atom. The ($\bar{2}$ 2 13.5) position was also measured simultaneously, and the X-ray voltammograms for that position are shown in Figure S7. These confirm that the onset of Pt extraction is independent of sweep rate.

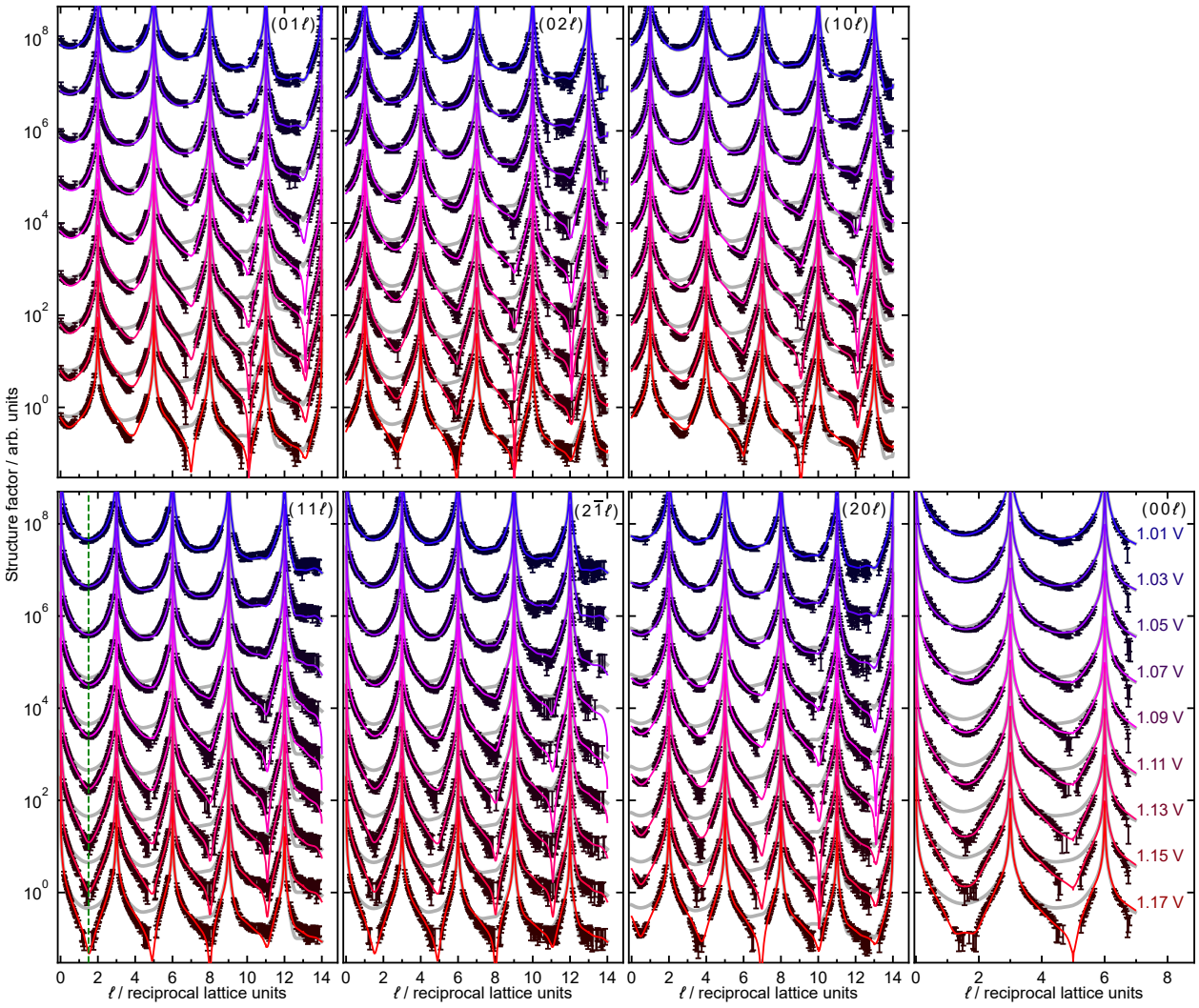

Figure S1: Crystal truncation rods, measured at different potentials in the initial stages of Pt oxidation. Solid colored lines are CTR fits with the oxide structural model illustrated in Figure 2b. As a reference the CTR fit at 1.01 V is shown together with the CTRs as solid gray lines. The structural parameters obtained from the fit are shown in Table S1.

Table S1: Structural parameters from CTR fits by the model shown in Figure 2b of the main manuscript. θ_{ex} is the coverage of Pt_{ex} atoms, d_{ex} and d_O are vertical distances of Pt_{ex} and O atoms above the plane of the surface (Pt1) layer, and d_{12}, d_{23} and d_{34} are interplanar distances. $(\Delta r_x)_\perp$ and $(\Delta r_x)_\parallel$ are the out-of-plane and in-plane Debye-Waller parameters of the corresponding x atoms.

E_{RHE}	1.01 V	1.03 V	1.05 V	1.07 V	1.09 V
θ_{ex}/ML	0.014(6)	0.017(6)	0.080(4)	0.136(5)	0.179(4)
d_{ex}/Å	2.05(4)	2.01(4)	2.096(25)	2.053(28)	2.075(21)
d_O/Å	2.23(4)	2.25(4)	1.340(27)	1.289(27)	1.233(22)
d_{12}/Å	2.2906(9)	2.2877(9)	2.2779(9)	2.2580(9)	2.2457(10)
d_{23}/Å	2.2764(7)	2.2779(7)	2.2793(7)	2.2809(7)	2.2821(8)
d_{34}/Å	2.2727(5)	2.2731(5)	2.2729(5)	2.2739(5)	2.2748(5)
$(\Delta r_{ex})_\parallel$/Å	0.18(11)	0.23(8)	0.343(22)	0.353(16)	0.355(12)
$(\Delta r_O)_\parallel$/Å	0.25(5)	0.25(5)	0.25(4)	0.25(5)	0.25(5)
$(\Delta r_1)_\parallel$/Å	0.076(4)	0.083(4)	0.081(4)	0.0871(30)	0.0977(29)
$(\Delta r_2)_\parallel$/Å	0.0761(26)	0.0766(26)	0.0756(25)	0.0754(26)	0.0755(27)
$(\Delta r_3)_\parallel$/Å	0.0759(23)	0.0758(22)	0.0756(21)	0.0754(22)	0.0754(22)
$(\Delta r_{ex})_\perp$/Å	0.12(6)	0.11(6)	0.235(24)	0.352(25)	0.355(19)
$(\Delta r_O)_\perp$/Å	0.24(5)	0.24(4)	0.23(4)	0.24(5)	0.22(5)
$(\Delta r_1)_\perp$/Å	0.1062(7)	0.1073(7)	0.1064(7)	0.1059(9)	0.1027(10)
$(\Delta r_2)_\perp$/Å	0.0952(7)	0.0961(6)	0.0950(6)	0.0940(7)	0.0948(7)
$(\Delta r_3)_\perp$/Å	0.0789(7)	0.0794(7)	0.0787(7)	0.0782(7)	0.0787(7)
R-factor	0.099	0.1	0.102	0.107	0.114
χ^2_r	1.17	1.19	1.21	1.14	1.28

E_{RHE}	1.11 V	1.13 V	1.15 V	1.17 V
θ_{ex}/ML	0.2220(24)	0.2578(19)	0.2625(20)	0.2987(18)
d_{ex}/Å	2.094(17)	2.156(13)	2.205(14)	2.212(13)
d_O/Å	1.202(25)	1.12(4)	1.09(4)	1.00(4)
d_{12}/Å	2.2391(11)	2.2324(12)	2.2292(13)	2.2202(15)
d_{23}/Å	2.2839(9)	2.2852(9)	2.2871(10)	2.2904(10)
d_{34}/Å	2.2744(5)	2.2754(6)	2.2765(6)	2.2763(7)
$(\Delta r_{ex})_\parallel$/Å	0.354(10)	0.353(10)	0.355(10)	0.349(9)
$(\Delta r_O)_\parallel$/Å	0.25(5)	0.25(5)	0.24(5)	0.24(4)
$(\Delta r_1)_\parallel$/Å	0.1084(30)	0.118(4)	0.126(4)	0.137(4)
$(\Delta r_2)_\parallel$/Å	0.0756(29)	0.076(4)	0.076(4)	0.079(4)
$(\Delta r_3)_\parallel$/Å	0.0755(23)	0.0755(24)	0.0755(25)	0.0756(26)
$(\Delta r_{ex})_\perp$/Å	0.355(16)	0.355(14)	0.355(14)	0.355(13)
$(\Delta r_O)_\perp$/Å	0.23(6)	0.25(6)	0.24(5)	0.23(5)
$(\Delta r_1)_\perp$/Å	0.0983(12)	0.0973(15)	0.0975(16)	0.0984(18)
$(\Delta r_2)_\perp$/Å	0.0964(7)	0.0967(8)	0.0972(9)	0.0982(10)
$(\Delta r_3)_\perp$/Å	0.0787(8)	0.0759(8)	0.0767(8)	0.0762(9)
R-factor	0.123	0.129	0.131	0.133
χ^2_r	1.43	1.53	1.82	1.9

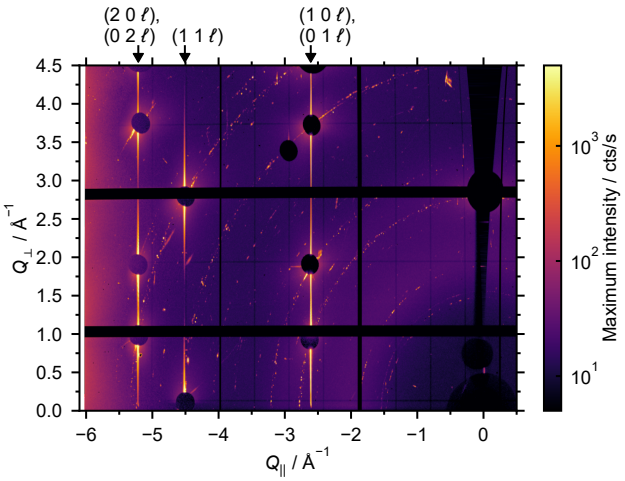

Figure S2: Reciprocal space map at 1.15 V, obtained from the HESXRD rocking scan. The CTRs are vertical lines, which are marked at the top of the image. The Bragg reflections of the Pt(111) crystal were covered by cylindrical beam stops and appear as circular black spots. No super lattice rods from a periodic oxide structure with a high-order commensurate surface lattice or incommensurate surface lattice are observed. The additional diffraction spots along rings most likely originate from polycrystalline areas on the sides of the Pt crystal. The reciprocal space map was obtained by combining all images from this measurement and showing the maximum intensity observed at each pixel. Only a selected fraction of the detector area close to $\ell = 0$ is shown for clarity.

Analysis of the Pt(111) oxide structure

The oxide structure of Pt(111) in the initial stages of oxidation is well established by now and multiple groups have analysed the Pt(111) oxide structure on the basis of CTR structure factor measurements.[S5–S8,S13,S14] However, all of the CTR measurements in the literature were restricted to a maximum vertical momentum transfer of $\ell < 7$, while the CTR data presented here extend over range of $\ell < 14$. Hence, the existing model of the Pt(111) oxide structure in the initial stages of oxidation needs to be verified for this higher vertical momentum transfer.

In agreement with previous works,[S6,S8] no in-plane diffraction features such as super lattice rods from a laterally ordered oxide structure were observed during any of the reciprocal space mappings for the CTR measurements between 1.01 V and 1.17 V. As an example, the reciprocal space map obtained during the CTR measurement at 1.15 V is shown in Figure S2. This indicates that the Pt_{ex} are either not arranged in a periodic lattice or that its domain

size is very small. The structural analysis therefore exclusively relies on the CTR structure factor. The CTR structure factors for several potentials between 1.01 V and 1.17 V are given in Figure S1.

Figure S1 also shows best fits of the CTRs by the Pt extraction model illustrated in Figure 2b. Although this model is well-established in the literature, we reinvestigated this by performed CTR fits where the Pt_{ex} atoms were placed at different high-symmetry in-plane positions, including the atop position. Pt surface atoms were allowed to vertically relax until the Pt3 layer (see Figure 2b for an illustration of the fitted vertical distances) and their corresponding in-plane and out-of-plane Debye-Waller parameters were fitted as well as the Pt_{ex} coverage. The Pt_{ex} coverage was coupled with the number of vacancies in the Pt1 layer (see Figure 2b) so that for each extracted Pt_{ex} a corresponding vacancy is left behind in the Pt surface. According to this analysis, CTR fits with the Pt_{ex} in atop positions were better than random roughness models, in which the Pt_{ex} are either localized in fcc hollow sites or are laterally disordered as in an amorphous oxide. We can therefore confirm that the Pt(111) oxide in the initial stages of oxidation is described by the structural model that was developed in previous SXRD studies.[S6–S8]

Most of the previous studies have also attempted to determine the location of the oxygen atoms in the oxide, but concluded that the scattering from oxygen is too weak to determine its precise position. A high coverage of oxygen in the form of 0.5 ML OH_{ads} is generally thought to be adsorbed in the butterfly peak around 0.65 V prior to surface oxidation.[S15] This coverage is expected to increase once the surface is oxidized. To assess the influence of the scattering from the oxygen on structural parameters such as the Pt_{ex} coverage obtained from the CTR analysis, we performed additional CTR fits with three structural models with different oxygen coverages. In all models, an equal amount of oxygen was placed in either fcc or hcp hollow sites as predicted by DFT calculations of the surface structure prior to surface oxidation.[S11,S12] The oxygen is also expected to be close to these locations after Pt extraction.[S11] CTR fits with either a fixed oxygen coverage of 1 ML or without any oxygen

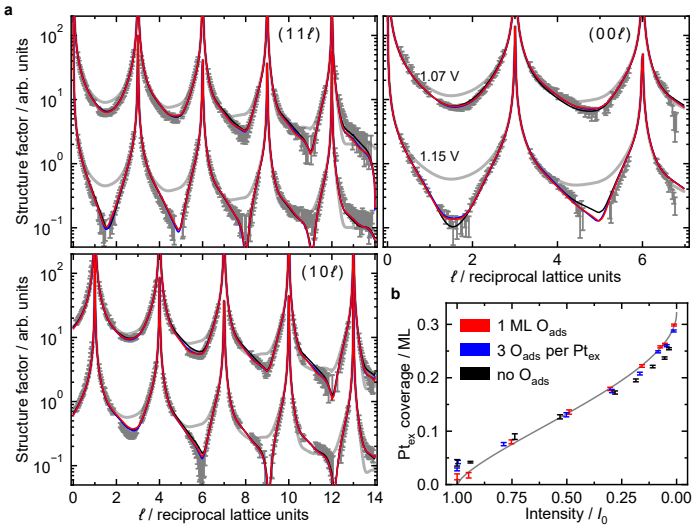

Figure S3: Influence of O_{ads} on CTR fits and the relation between structure factor and Pt_{ex} coverage. (a) Selected CTRs at 1.05 and 1.15 V and fits with either 1 ML O_{ads} (red), 0 ML O_{ads} (black), or 3 O_{ads} per Pt_{ex} atom (blue). As a reference, the CTR fit of the oxide-free surface at 1.01V is shown (gray). (b) Relation between intensity at (1 1 1.5) and Pt_{ex} coverage for the different O_{ads} coverage models. The position of the data points on the intensity axis varies, since the intensity from the CTR fits is used for this relation. The solid grey line is the empirical fit to this relation used to calculate the Pt_{ex} coverage in Figure 1d, S4, and S6.

adsorbate, an extreme but rather unrealistic case, are shown in Figure S3a. Additionally, CTR fits are shown where three oxygen atoms are added per extracted Pt (i.e., the minimum amount of stabilizing oxygen obtained from DFT calculations[S11,S12]), representing a model with an increasing oxygen coverage upon surface oxidation. All CTR fits are very similar, showing that the scattering from the oxygen can be compensated by a small variation of the location and coverage of the Pt atoms. The relation between the calculated intensity at (1 1 1.5) and the Pt_{ex} coverage obtained from these three models is shown in Figure S3b. The influence of the oxygen is clearly minor, apart from the case of the oxide-free surface (Pt_{ex} coverage ≈ 0 ML) where the omission of the adsorbed 0.5 ML OH enforces a residual Pt_{ex} coverage. Otherwise, the error due to the unknown oxygen coverage, estimated from the model with the minimum number of 3 stabilizing oxygen per Pt_{ex}, is below ± 0.025 ML. The latter should be added to the error bars in Figure S4a and S6 for a better estimation of the error of the absolute Pt_{ex} coverage. However, for a comparison of the measurements with different sweep rates, where relative changes are compared, the presented statistical errors

are more relevant.

Relationship of extracted coverages to potential

The coverages as a function of potential in the forward sweeps (data in Figure 1d) were fitted to the electrochemical Langmuir isotherm, equation (1)

$$\theta_{\mathrm{ex}}(E) = \frac{\theta_{\mathrm{ex,s}}}{1 + \exp(-b(E - E^{\circ}))} \tag{1}$$

where $\theta_{\mathrm{ex,s}}$ is the saturation coverage (ML), E° is the standard potential, and b is an energy parameter. Fits are shown in Figure S4a and the fitted parameters are shown as a function of potential in Figure S4b. The standard potentials range over 16 mV from 1.098 V to 1.114 V, but given the error bars and lack of obvious trend, there does not seem to be any significant shift in the curves. This standard potential for the extraction is close to the thermodynamic value 1.06 V calculated by DFT for Pt extraction (at a coverage of 0.7 ML O_{ads}).[S1]

The energy parameter shows no potential dependence and has a value $b = 43.5 \pm 1.3\,\mathrm{V}^{-1}$ corresponding to $(1.116 \pm 0.033)F/RT$. Here the quoted values and errors are from a global fit in which only the saturation coverages were allowed to vary with potential.

The saturation coverages, $\theta_{\mathrm{ex,s}}$ showed some small sweep rate dependence and were in the range 0.14 – 0.18 ML, indicating some kinetic influence already on the forward sweep.

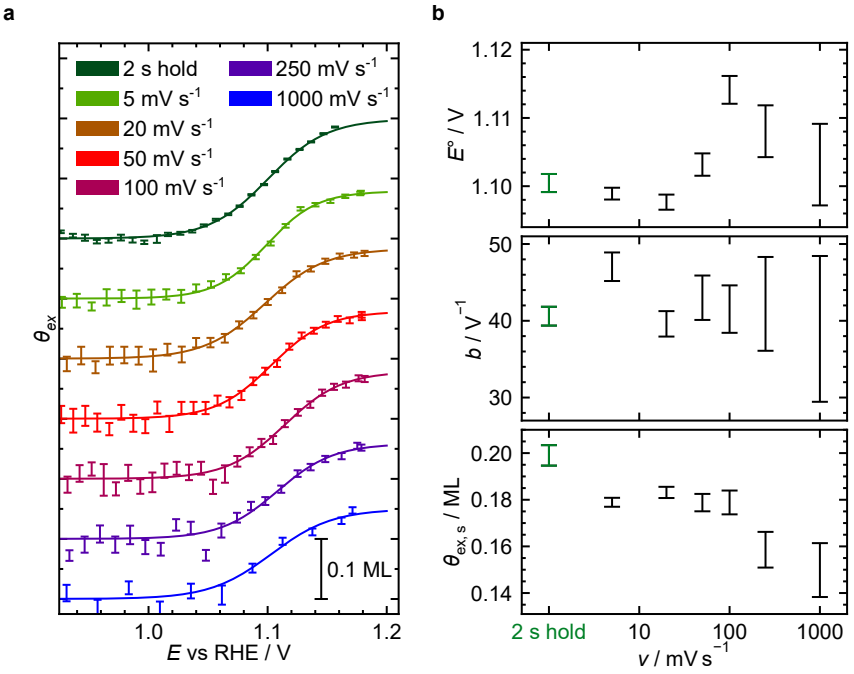

Figure S4: Quantitative description of the coverage of extracted Pt atoms as a function of potential. (a), Experimental $\theta_{\mathrm{ex}}(E)$ curves obtained from CVs at different sweep rates together with fits by the quasi-equilibrium model (solid lines). Also shown are θ_{ex} 2 s after potential steps to E, from step data shown and described in Figure S8. The curves are offset by 0.1 ML with respect to each other. (b), standard potential E°, energy parameter b and saturation coverage $\theta_{\mathrm{ex,s}}$ obtained from the fits. The fit parameters obtained 2 s after potential steps are shown as green data arbitrarily placed at 1 mV s^{-1}.

Cyclic voltammograms and potential step transients

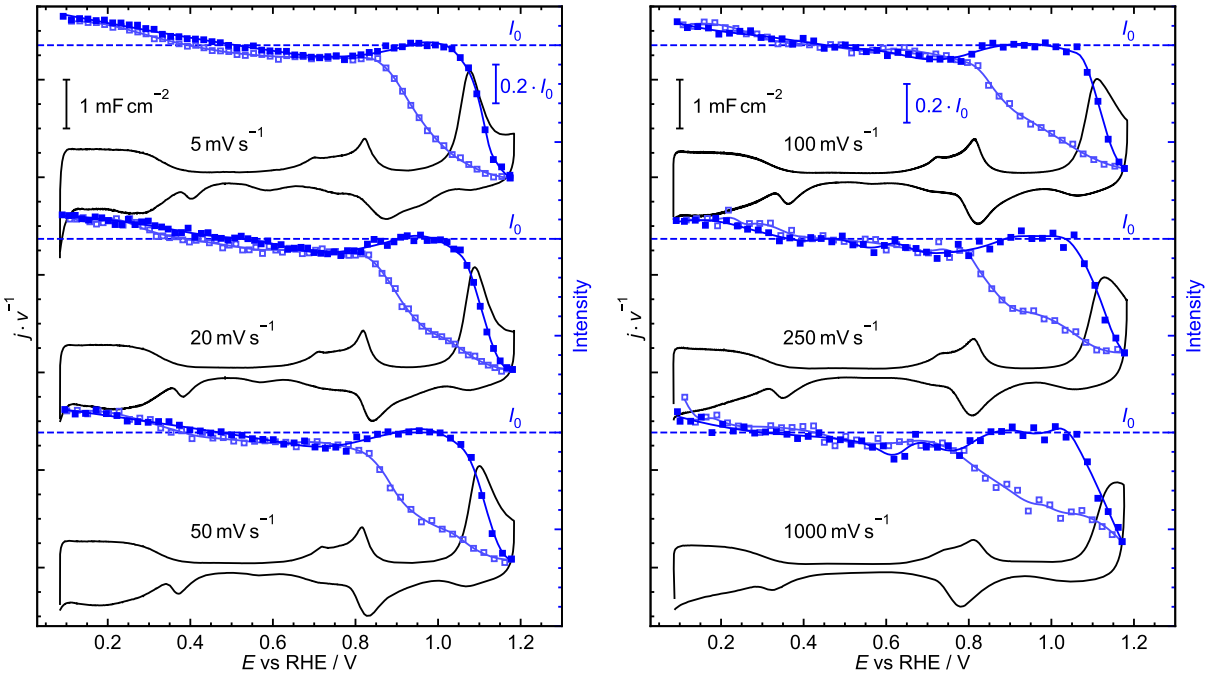

Figure S5: Cyclic voltammograms and simultaneously measured X-ray intensity at (1 1 1.5). The intensity of the first forward sweep is shown as filled blue squares, the intensity of the reverse sweep is shown as empty blue squares.

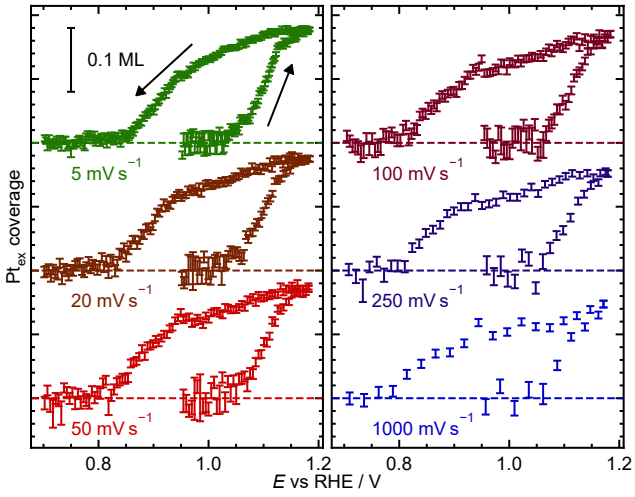

Figure S6: Coverage of extracted Pt atoms during potential cycling. The coverage was obtained from the X-ray intensity at (1 1 1.5) in Figure S5 using the the relation shown in Figure 2c and S3b. The cycling direction is indicated with black arrows. Pt_{ex} coverage obtained with different sweep rates are offset by 0.2 ML with respect to each other. A dashed horizontal line indicates the position of 0 ML for each data set.

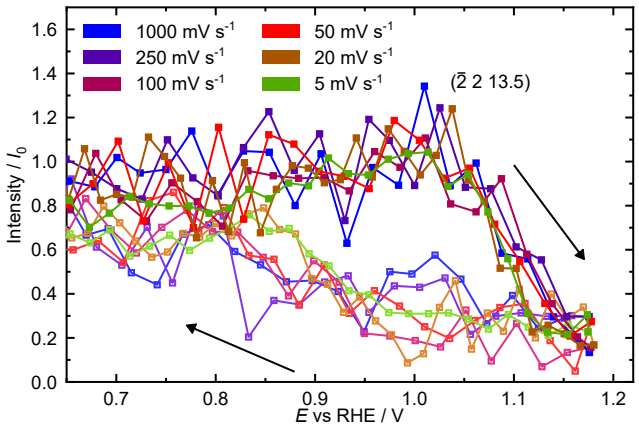

Figure S7: X-ray intensity at the ($\bar{2}$ 2 13.5) position during potential cycling. The intensity of the forward sweep is shown as filled squares, the intensity of the reverse sweep is shown as empty squares. The ($\bar{2}$ 2 13.5) reflection is equivalent to (2 0 13.5) in Figure S1.

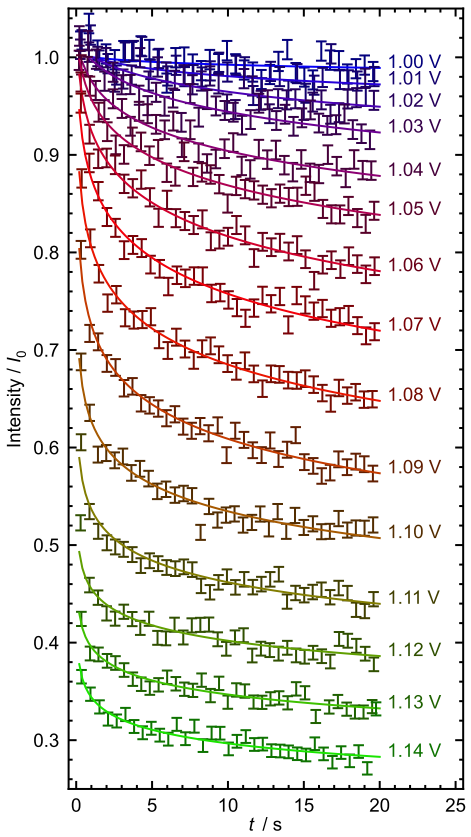

Figure S8: X-ray intensity after potential steps. Intensity at (1 1 1.5) for successive steps from the double-layer (0.47 V) to the indicated potentials. After 20 s at that potential, the potential was help for 5 s at 0.47 V before the next step. The θ_{ex} values in Figure S4 were obtained from the average intensity between 1 and 3 s.

References

(S1) Fuchs, T.; Drnec, J.; Calle-Vallejo, F.; Stubb, N.; Sandbeck, D. J. S.; Ruge, M.; Cherevko, S.; Harrington, D. A.; Magnussen, O. M. Structure dependency of the atomic-scale mechanisms of platinum electro-oxidation and dissolution. *Nat. Catal.* **2020**, *3*, 754–761.

(S2) Magnussen, O. M.; Krug, K.; Ayyad, A. H.; Stettner, J. In situ diffraction studies of electrode surface structure during gold electrodeposition. *Electrochim. Acta* **2008**, *53*, 3449–3458.

(S3) Wang, J.; Ocko, B.; Davenport, A.; Isaacs, H. In situ X-ray-diffraction and -reflectivity studies of the Au(111)/electrolyte interface: reconstruction and anion adsorption. *Phys. Rev. B* **1992**, *46*, 10321–10338.

(S4) Gustafson, J.; Shipilin, M.; Zhang, C.; Stierle, A.; Hejral, U.; Ruett, U.; Gutowski, O.; Carlsson, P.-A.; Skoglundh, M.; Lundgren, E. High-energy surface X-ray diffraction for fast surface structure determination. *Science* **2014**, *343*, 758–761.

(S5) You, H.; Zurawski, D. J.; Nagy, Z.; Yonco, R. M. In-situ x-ray reflectivity study of incipient oxidation of Pt(111) surface in electrolyte solutions. *J. Chem. Phys.* **1994**, *100*, 4699–4702.

(S6) Drnec, J.; Ruge, M.; Reikowski, F.; Rahn, B.; Carlà, F.; Felici, R.; Stettner, J.; Magnussen, O. M.; Harrington, D. A. Initial stages of Pt(111) electrooxidation: dynamic and structural studies by surface X-ray diffraction. *Electrochim. Acta* **2017**, *224*, 220–227.

(S7) Ruge, M.; Drnec, J.; Rahn, B.; Reikowski, F.; Harrington, D.; Carlà, F.; Felici, R.; Stettner, J.; Magnussen, O. Electrochemical oxidation of smooth and nanoscale rough Pt(111): An in situ surface X-ray scattering study. *J. Electrochem. Soc* **2017**, *164*, H608–H614.

(S8) Jacobse, L.; Vonk, V.; McCrum, I. T.; Seitz, C.; Koper, M. T.; Rost, M. J.; Stierle, A. Electrochemical oxidation of Pt(111) beyond the place-exchange model. *Electrochim. Acta* **2022**, *407*, 139881.

(S9) Sandbeck, D. J.; Brummel, O.; Mayrhofer, K. J.; Libuda, J.; Katsounaros, I.; Cherevko, S. Dissolution of platinum single crystals in acidic medium. *ChemPhysChem* **2019**, *20*, 2997–3003.

(S10) Lopes, P. P.; Strmcnik, D.; Tripkovic, D.; Connell, J. G.; Stamenkovic, V.; Markovic, N. M. Relationships between atomic level surface structure and stability/activity of platinum surface atoms in aqueous environments. *ACS Catal.* **2016**, *6*, 2536–2544.

(S11) Eslamibidgoli, M. J.; Eikerling, M. H. Atomistic mechanism of Pt extraction at oxidized surfaces: Insights from DFT. *Electrocatalysis* **2016**, *7*, 345–354.

(S12) Fantauzzi, D.; Mueller, J. E.; Sabo, L.; van Duin, A. C. T.; Jacob, T. Surface buckling and subsurface oxygen: atomistic insights into the surface oxidation of Pt(111). *ChemPhysChem.* **2015**, *16*, 2797–2802.

(S13) Nagy, Z.; You, H. Applications of surface X-ray scattering to electrochemistry problems. *Electrochim. Acta* **2002**, *47*, 3037–3055.

(S14) Liu, Y.; Barbour, A.; Komanicky, V.; You, H. X-ray crystal truncation rod studies of surface oxidation and reduction on Pt(111). *J. Phys. Chem. C* **2016**, *120*, 16174–16178.

(S15) Gómez-Marín, A. M.; Feliu, J. M. Pt(111) surface disorder kinetics in perchloric acid solutions and the influence of specific anion adsorption. *Electrochim. Acta* **2012**, *82*, 558–569.